



FRONTIERS ARTICLE

The Chiral Plaquette Polaron Paradigm (CPPP) for high temperature cuprate superconductors

Jamil Tahir-Kheli *, William A. Goddard III *

Materials and Process Simulation Center (MC 139-74), California Institute of Technology, Pasadena, CA 91125, United States

ARTICLE INFO

Article history:

Received 14 January 2009

In final form 10 February 2009

Available online 13 February 2009

ABSTRACT

A scientific revolution occurred in 1986–1994 in which the T_c for the best superconductors exploded from 23 K (Nb₃Ge) to 138 K (Hg_{0.2}Tl_{0.8}Ba₂Ca₂Cu₃O_{8.33}). Despite enormous effort over the last 21 years, the superconducting mechanism remains unknown. All previous attempts assumed that the doped holes were in the CuO₂ plane. We showed recently with improved quantum mechanics (QM) calculations that *the hole is out of the CuO₂ plane* and delocalized over four Cu atoms in a square **Plaquette** that forms the basis of our **Chiral Plaquette Polaron Paradigm (CPPP)**. Here, we show how very simple geometric arguments provide a qualitative understanding of the broad range of cuprate phenomenology. This simple geometric analysis may be useful in guiding the development of materials for improved superconductors. The CPPP suggests that judicious control of the dopant distribution could possibly lead to a room-temperature T_c .

© 2009 Elsevier B.V. All rights reserved.

1. Introduction

The discovery of superconductivity in Mercury ($T_c = 4.2$ K) in 1911, was followed by Lead ($T_c = 6$ K) in 1912, Nb ($T_c = 9.25$ K) in 1930, NbN ($T_c = 16.1$ K) in 1941, Nb₃Sn ($T_c = 18.1$ K) in 1954, and Nb₃Ge ($T_c = 23.2$ K) in 1971 [1]. This slow evolution seemed to be converging to the fundamental limit of ~ 30 K suggested by Morel and Anderson for phonon pairing [2]. Thus, the unanticipated discovery of a cuprate superconductor with $T_c = 35$ K in La_{2-x}Ba_xCuO₄ by Bednorz and Muller in 1986 [3] led to an unprecedented explosion of materials and record-breaking T_c 's with 38 K for La_{2-x}Sr_xCuO₄ in 1987, 92 K for YBa₂Cu₃O₇ in 1987, and finally culminating in (Hg_{0.2}Tl_{0.8})Ba₂Ca₂Cu₃O_{8.33} with 138 K in 1993. This increase of T_c by 115 K took place in just 6 years. Unfortunately, for the past 15 years, the maximum T_c has not budged. We believe that this is because there has been no sound theoretical basis for understanding the current materials that could be used as a guidepost in suggesting new materials and structures.

This punctuated evolution of the highest T_c superconducting materials has resulted from serendipitous discovery of new material classes, followed by rapid experimental optimization. Theory has played virtually no role in this process. Indeed, it took 46 years to develop the theory underlying the superconductivity of Hg and Pb (discovered in 1911) and explained in 1957 [by Bardeen, Cooper, and Schrieffer (BCS)] [4].

Since 1986 there have been tens of thousands of theory papers on the cuprates, yet no theory is generally accepted by the community and none has successfully suggested a way to systematically improve these materials. The world has already waited half the 46 years it took for BCS to explain classical superconductors. Hopefully, we will not have to wait another 23 to understand the cuprates.

The challenge of explaining cuprate superconductivity goes far beyond merely understanding the mechanism of the pairing interaction that leads to increased T_c because the transport properties for the normal (non-superconducting) state of the cuprates are also anomalous. In classical BCS superconductors, the normal state properties are consistent with the standard concepts of a Fermi surface, density of states, and a temperature dependent scattering rate. Thus, the breakthrough of BCS was to find the correct ground state and excitations for the superconducting phase. No new concepts were required to explain the normal phase properties.

In contrast, a correct theory of the cuprates must simultaneously explain why superconductivity occurs, the nature of the pairing, the observed superconducting $d_{x^2-y^2}$ gap symmetry (called D-wave) where the x - and y -axes are along the planar Cu–O bond directions, the high T_c , the doping phase diagram, and the numerous anomalies observed in the electronic and magnetic transport properties of the normal state above T_c . These anomalies extend over the complete range of doping for which the cuprates are superconductors.

We believe understanding the ‘anomalous’ normal state transport properties of cuprates is an extremely important problem in itself because one might be able to modify or enhance these properties to create new types of devices coupling electronic, magnetic,

* Corresponding authors. Fax: +1 626 585 0918.

E-mail addresses: jamil@wag.caltech.edu (J. Tahir-Kheli), wag@wag.caltech.edu (W.A. Goddard III).

transport, and thermodynamic characteristics. Thus, understanding the cuprates could have a dramatic effect on solid-state materials design—beyond just superconducting materials.

In this Letter, we summarize a new paradigm for understanding the superconducting and transport properties of the cuprates based firmly on the best available quantum mechanics (QM) calculations. We find that the **holes** induced by the doping and responsible for superconductivity involve Cu d orbitals and oxygens that are **out of the CuO₂ plane** and **delocalized over a square site involving four Cu atoms** that we call the **Plaquette**. Here, we focus on key aspects of this new theory with an emphasis on some simple geometric features that could be useful to non-theorists to suggest compositions and structures that might lead to higher T_c materials.

We emphasize here that the conclusion that the holes responsible for the unique properties of cuprates are out-of-the-plane orbitals, directly contradicts the consensus opinion in this field that was summarized by Anderson in his 1997 book, *The Theory of Superconductivity in the High- T_c Cuprates* [5]. In his ‘Central Dogmas’ in Chapter 2, he states:

Dogma I: All the relevant carriers of both spin and electricity reside in the CuO₂ planes and derive from the hybridized O2p-dx₂y₂ orbital which dominates the binding in these compounds. . . Dogma I in summary: look at the planes only (a great and welcome simplification).

In addition, our paradigm violates Anderson’s second central dogma:

Dogma II: Magnetism and high- T_c superconductivity are closely related, in a very specific sense: i.e., the electrons which exhibit magnetism are the same as the charge carriers.

This is described in Section 4.1. Despite the failure of Anderson’s inter-layer tunneling theory [6] that formed the basis of his book [5], ‘Dogma I’ is still generally believed to be correct.

In Section 2 we summarize the main structural characteristics of cuprates and the assumptions about the effects of doping. Section 3 brings in the results from the newer QM showing that the holes are out of the CuO₂ plane and in the vicinity of the dopants. Section 4 lists the fundamental assumptions of the CPPP and Section 5 shows how CPPP explains a broad spectrum of experiments. In order to provide a basis for non-theorists to understand the concepts well enough to use them in thinking about new materials, we have attempted to keep the arguments qualitative even when more quantitative calculations are available. Section 6 uses CPPP to estimate the maximum possible T_c (150–450 K). Section 7 presents our conclusions.

2. Cuprate structures and the effect of doping

2.1. Summary of crystal structures

The cuprate superconductivity era began with the discovery in late 1986 by Bednorz and Muller [3] of superconductivity at 35 K in La_{2-x}Ba_xCuO₄ (LBCO), which is based on the perovskite crystal structure. High temperature superconductivity has since been discovered in several other classes of materials, La_{2-x}Sr_xCuO₄ (LSCO) with T_c up to 38 K, YBa₂Cu₃O_{7-δ} (YBCO) with T_c up to 92 K, Bi₂Sr₂Ca_{n-1}Cu_nO_{4+2n} (BiSCCO) with T_c up to 110 K, TlBa₂Ca_{n-1}Cu_nO_{3+2n} with T_c up to 123 K, Tl₂Ba₂Ca_{n-1}Cu_nO_{4+2n} with T_c up to 112 K, and the current reigning high T_c champion discovered in 1993, (Hg_{0.2}Tl_{0.8})Ba₂Ca₂Cu₃O_{8.33} with T_c = 138 K. These materials are hole-doped relative to the undoped antiferromagnetic (AF) material. There are some electron-doped cuprate superconductors such as Nd_{2-x}Ce_xCuO_{4-δ} and Sr_{1-x}La_xCuO₂ (T_c = 90 K). However, the

exact location of the dopant atoms is uncertain with the electron-doped materials, making it more complicated to examine than the hole-doped systems. Thus it is not known whether the charge carriers in the CuO₂ planes are electrons or holes. We will not discuss them here.

The undoped parent structures of cuprate superconductors are insulating and antiferromagnetic, but not superconducting. In La_{2-x}Ba_xCuO₄ and La_{2-x}Sr_xCuO₄, the parent compound is La₂CuO₄, shown in Fig. 1a. La₂CuO₄ is a spin-1/2 Heisenberg AF with an exchange coupling of $J_{dd} = 0.13$ eV [7]. The Néel temperature, or AF ordering temperature, of $T_N = 325$ K arises from the small (~1 K) exchange coupling between CuO₂ planes since a true 2D Heisenberg AF has $T_N = 0$ [8].

Superconductivity arises through doping, but the doping can take several forms. In La_{2-x}Sr_xCuO₄, the doping is due to Sr substitution at La sites, leading to a deficit of electrons (hole doping). In other cuprates, the doping arises from O defects. Thus in YBa₂Cu₃O_{7-δ} (shown in Fig. 1b) the undoped AF parent compound, $\delta = 1$, has no O atoms in the Cu–O chains, while the limiting case of $\delta = 0$ would have 1 hole per every three Cu (or one per chain Cu). In other systems, such as Bi₂Sr₂CaCu₂O_{8+δ}, the additional O atoms leading to hole doping probably reside in locations away from the CuO₂ planes, but serve to remove electrons associated with the planes.

The characteristic common to all cuprate superconductors is the existence of CuO₂ planes, as seen in Fig. 2a, in which Cu^{II} d⁹ atoms are in a square of side ~3.86 Å and connected through O atoms (~1.93 Å bond distances) with linear Cu–O–Cu. These in-plane Cu atoms may have zero, one, or two axial O neighbors (at ~2.4 Å). In LBCO and LSCO, the CuO₂ planes are isolated. YBCO and Bi₂Sr₂CaCu₂O_{8+δ} (Bi-2212) have two adjacent CuO₂ planes, while Bi-2223 has three adjacent CuO₂ planes. T_c typically (but not always) increases as the number of adjacent CuO₂ layers increases up to three, and then decreases.

Fig. 2b shows the spin-1/2 AF structure of a single CuO₂ plane for the undoped parent compounds. Each Cu atom is in the II oxidation state leading to a d⁹ electronic configuration, with the lobes of the singly-occupied d_{x₂-y₂} orbital pointing toward the four O

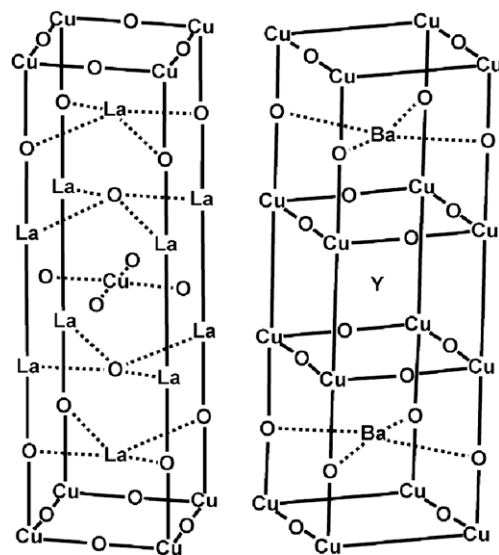


Fig. 1. The crystal structures for La₂CuO₄ and YBa₂Cu₃O_{7-δ} (with $\delta = 0$). The former is the undoped parent compound of the La_{2-x}(Sr,Ba)_xCuO₄ superconductors. It is a spin-1/2 antiferromagnet with localized spins on the Cu d⁹ sites in a singly occupied d_{x₂-y₂} orbital. The Heisenberg spin–spin coupling (see Eq. (1)) is $J_{dd} = 0.13$ eV. The latter is a superconductor with $T_c = 92$ K. The undoped antiferromagnet for the YBaCuO system occurs for $\delta = 1$. The O defects in YBCO occur in the one-dimensional Cu–O chains.

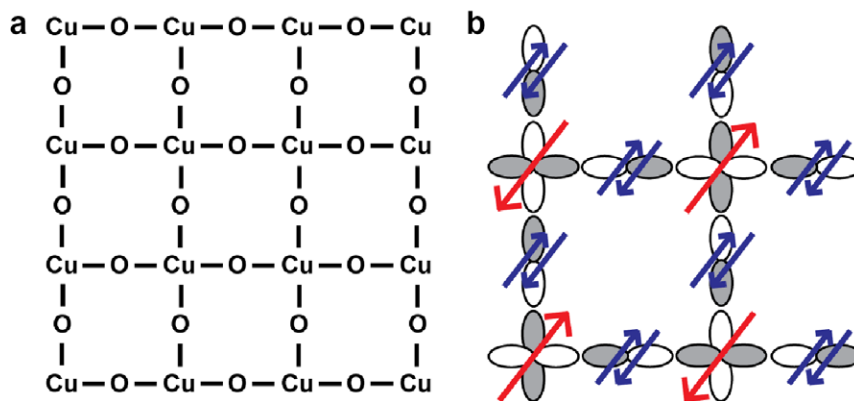


Fig. 2. (a) The CuO_2 plane characteristic of all cuprate superconductors. (b) The localized spin configuration for the CuO_2 plane in an undoped antiferromagnetic cuprate. The singly occupied spin on the Cu atom is in the $d_{x^2-y^2}$ orbital with the lobes pointing along the Cu–O bond direction. The $O_{p\sigma}$ orbital is doubly occupied.

atoms in the sheet (~ 1.93 Å bond distance). The remaining four Cu d orbitals (d_{xy} , d_{xz} , d_{yz} , d_{z^2}) are doubly occupied, leading to long bonds (~ 2.4 Å) to any out-of-plane O atoms. Describing each O as O^{2-} , we will denote the 3 doubly occupied O p orbitals as: $p\sigma$ (pointing toward the Cu atom), $p\pi$ (in the plane but perpendicular to the Cu–O–Cu bond), and p_z (perpendicular to the CuO_2 plane). These are doubly occupied in the undoped systems. The states of the undoped system are well described by a Heisenberg Hamiltonian,

$$H_{dd} = J_{dd} \sum S_i \cdot S_j, \quad (1)$$

where $J_{dd} = 0.13$ eV for La_2CuO_4 .

The generic phase diagram of the cuprates is shown in Fig. 3, where the fraction of holes per Cu in the CuO_2 planes (denoted as x) is along the abscissa. For dopings of $x < 0.02$, the system remains AF with a Neel temperature that decreases sharply with doping. For $0.02 < x < 0.05$ the phase is a spin-glass with conduction that is likely dominated by localized hopping [9]. At $x \sim 0.05$ holes per Cu in the CuO_2 plane, the superconducting phase begins. The optimal T_c occurs at $x \sim 0.16$ doping and superconductivity disappears at $x \sim 0.27$ doping (but the material remains a metallic conductor).

The region in the phase diagram above T_c and below $x \sim 0.16$ exhibits some characteristics of a superconductor without actually leading to superconductivity. This is called the *pseudogap region*. This pseudogap region exhibits a suppression of the density of states at the Fermi energy that would be consistent with the existence of a superconducting gap. The pseudogap becomes zero above the dotted line in the figure. It is unknown whether the dotted line boundary is a true phase transition. The alternative is a smooth transition from finite to zero pseudogap across the dotted line over a narrow temperature range.

The nonsuperconducting ‘metallic’ state for all dopings is referred to as a ‘*strange metal*’ because it exhibits transport properties (temperature dependence of the resistivity, temperature dependence of the Hall effect, magnetoresistance, reflectance, mid-IR absorption, etc.) that are not consistent with conventional solid state theories of metals (Fermi liquid theory) [10,11]. We will discuss several of these transport properties below.

For $\text{La}_{2-x}\text{Sr}_x\text{CuO}_4$, each Sr introduces exactly one hole into the material. Since all Cu atoms are in the CuO_2 plane, the x in $\text{La}_{2-x}\text{Sr}_x\text{CuO}_4$ corresponds exactly to the x -axis in Fig. 3.

Since $\text{YBa}_2\text{Cu}_3\text{O}_{7-\delta}$ has Cu atoms in chains and sheets, the doping in the planes (x) is a complicated function of the O defects (δ). For YBCO, it has been established that $\delta \approx 0.64$ corresponds to $x \sim 0.05$ hole doping in the planes, while optimal doping of $x \sim 0.16$ occurs for $\delta \approx 0.07$. Thus $\text{YBa}_2\text{Cu}_3\text{O}_7$ with completely full Cu–O chains is slightly overdoped.

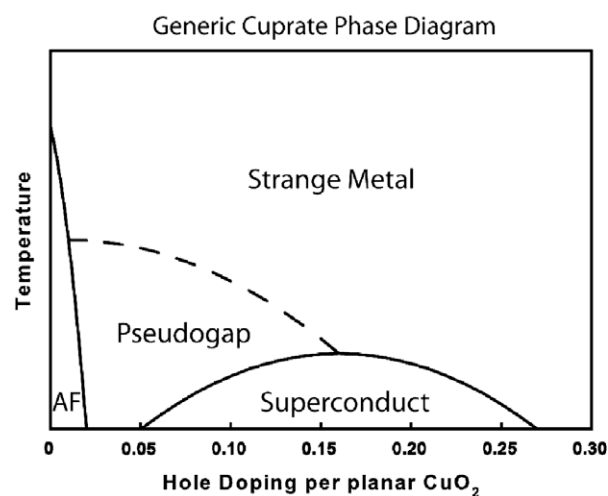


Fig. 3. The generic phase diagram for hole-doped cuprate superconductors. At very low doping, the system is an insulating antiferromagnet. For dopings between 0.05 and 0.27, the superconducting phase appears. The dotted line shows the region for the so-called pseudogap phase. In this region, it appears as if a non-zero superconducting gap has opened without superconductivity. The pseudogap disappears for temperatures above the dotted line. It is unknown if there is a phase transition at the dotted line. The strange metal phase indicates that normal state transport properties for these systems differ from the form expected for a traditional metal with a Fermi surface, density of states, and a scattering rate (Fermi liquid). In the CPPP, the pseudogap is due to the AF coupling of the undoped d^9 spins to the metallic $x^2y^2/p\sigma$ band electrons. The anomalous transport in the strange metallic regime is due to interaction of the band electrons with the surface plaquettes. We find that at the highest dopings, the strange metallic phase becomes closer to that expected for a normal metal. This occurs in PPP because the interior plaquette states lead to normal Fermi liquid behavior and the number of surface plaquettes relative to the size of the metallic region goes to zero.

2.2. Effect of doping

The first CuO cluster calculations (Cu_3O_{10} plus ~ 1000 point charges to adjust the Madelung potential) using the Generalized Valence Bond (GVB) method found two low lying states both with holes on the O ($O_{p\sigma}$ and $O_{p\pi}$ to form O^-), as shown in Fig. 4a–c [12].

2.2.1. The $O_{p\pi}$ hole

For the state with the $O_{p\pi}$ orbital singly occupied, the favored spin coupling of this $O_{p\pi}$ orbital with the Cu $d_{x^2-y^2}$ orbitals on the two adjacent Cu atoms is ferromagnetic, leading to a total spin $S = 3/2$ quartet. This is because $O_{p\pi}$ is orthogonal to the Cu $d_{x^2-y^2}$ orbitals. This causes the spin of one Cu to be flipped (blue arrow

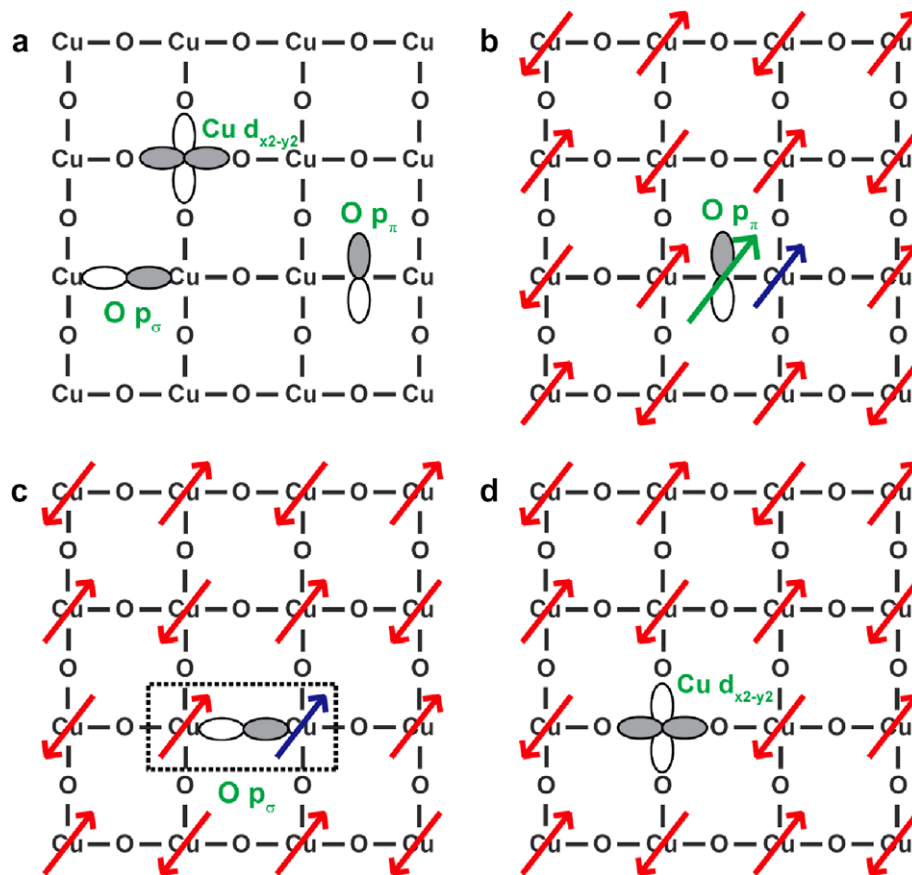


Fig. 4. (a) Plausible positions for holes in the CuO_2 plane. Here $\text{O}_{p\sigma}$ and $\text{O}_{p\pi}$ represent singly occupied orbitals (O^- rather than O^{2-}) that will have bonding or exchange interactions with the adjacent singly occupied $\text{Cu } d_{x^2-y^2}$ orbitals. On the other hand, a hole in the $\text{Cu } d_{x^2-y^2}$ orbital leads to zero electrons in this orbital, a $\text{Cu } d^8$ closed shell singlet state. (b) Since the $\text{O}_{p\pi}$ orbital is singly occupied but orthogonal to the singly occupied $\text{Cu } d_{x^2-y^2}$ orbitals on the two adjacent Cu atoms, the favored spin coupling is ferromagnetic, with total spin $S = 3/2$ or quartet. This leads to a resonating spin doublet ground state analogous to the pi system of the allyl radical, with the unpaired spin equally on Cu adjacent to the blue spin. For this $\text{O}_{p\pi}$ hole to hop to adjacent O sites, the spins on some of the various Cu atoms would have to flip. This was the basis of the magnon pairing theory of superconductivity [13–15], which led to triplet Cooper pairing that is inconsistent with observed singlet pairs [16–18]. This indicates that the $\text{O}_{p\pi}$ hole is not the ground state for the doped system. (c) The GVB calculations on CuO clusters [12–15] found a covalent bond between a singly-occupied $\text{O}_{p\sigma}$ orbital with either adjacent singly occupied $\text{Cu } d_{x^2-y^2}$ orbitals of the two adjacent Cu atoms. This leads to a resonating spin doublet ground state analogous to the pi system of the allyl radical, with the unpaired spin equally on Cu $d_{x^2-y^2}$ orbitals of both adjacent Cu atoms (this is indicated by the dotted rectangle encircling both spins). This causes the spin of one Cu to be flipped (blue arrow) frustrating the normal d^9-d^9 AF interactions with Cu adjacent to the blue spin. For this $\text{O}_{p\sigma}$ hole to hop to adjacent O sites, the spins on some of the various Cu atoms would have to flip. This state with a singly occupied $\text{O}_{p\sigma}$ orbital can be considered as the basis for many discussions of superconductivity, such as the t - J model. (d) Here, we illustrate the other extreme of an electron removed from the $\text{Cu } d_{x^2-y^2}$ orbital, which leads to a singlet closed shell d^8 state of Cu^{III} . This was the basis for the Resonating Valence Bond (RVB) theory of superconductivity [24,25]. This localized state would not modify directly the spins of the adjacent copper atoms, but it would weaken the superexchange coupling leading to the antiferromagnetic ground state. However, for this hole to hop to adjacent Cu sites, the spins on some of the various Cu atoms would have to flip. Closed shell calculations of this state would lead to delocalization of the hole onto the B_{1g} combination of the four adjacent $\text{O}_{p\sigma}$ orbitals. This is referred to as the Zhang-Rice singlet and is the basis for the popular t - J model of superconductivity [29].

in Fig. 4b), frustrating the normal d^9-d^9 antiferromagnetic interactions with Cu adjacent to the blue spin. For this $\text{O}_{p\pi}$ hole to hop to adjacent O sites, the spins on some of the Cu atoms would have to flip. This was the basis of the magnon pairing theory of superconductivity developed in 1988 [13] by Goddard and coworkers. Later, they showed that this leads to a P-wave gap symmetry with triplet Cooper pairs [14,15]. By 1994, phase sensitive Josephson tunneling experiments determined that the gap has D-wave ($d_{x^2-y^2}$) symmetry [16–18] and the Cooper pairs form singlets. This is inconsistent with the magnon pairing theory and shows that the $\text{O}_{p\pi}$ state is not the ground state of the cuprates.

2.2.2. The $\text{O}_{p\sigma}$ hole

The GVB calculations on CuO clusters also found a second state in which a singly-occupied $\text{O}_{p\sigma}$ orbital is spin-paired (covalently bonded) to the singly occupied $\text{Cu } d_{x^2-y^2}$ orbital of one of the two adjacent Cu atoms. This leads to a resonating spin doublet ground state analogous to the pi system of the allyl radical, with the unpaired spin equally on Cu $d_{x^2-y^2}$ orbitals of both adjacent

Cu atoms (this is indicated by the dashed rectangle encircling both spins in Fig. 4c). This causes the spin of one Cu to be flipped (blue arrow in Fig. 4c), frustrating the normal d^9-d^9 antiferromagnetic interactions with Cu adjacent to the blue spin. For this hole to hop to adjacent O sites, the spins on some of the various Cu atoms would have to flip. This state with a singly occupied $\text{O}_{p\sigma}$ orbital can be considered as the basis for most discussions of superconductivity. However, in our analyses of the properties resulting from the state, we could not convince ourselves that it would lead to a superconductor [19–23]. The problem was that pairing due to the covalent binding between the $\text{O}_{p\sigma}$ and $\text{Cu } d_{x^2-y^2}$ orbitals seemed to stabilize a local spin polaron that made it difficult for the hole to hop to adjacent sites. Thus, neither state from the GVB calculations seemed to explain the superconducting properties.

A third possibility for the hole is the other extreme shown in Fig. 4d, in which an electron is removed from the $\text{Cu } d_{x^2-y^2}$ orbital. This leads to a singlet closed shell d^8 state of Cu^{III} , which was the original basis for the Anderson Resonating Valence Bond (RVB) theory

of superconductivity [24,25]. This localized state would not modify directly the spins of the adjacent copper atoms, but it would weaken the superexchange coupling responsible for the antiferromagnetic ground state. However, for this hole to hop to adjacent Cu sites, the spins on some of the various Cu atoms would have to flip. The GVB calculations indicated that this state was not stable, with the hole localizing on an adjacent $O_{p\sigma}$ to form a covalent bond.

2.2.3. The hole from band calculations and t - J models

Cluster calculations at the Hartree Fock and Density Functional Theory levels generally lead to delocalization of the bonding electrons between the Cu $d_{x^2-y^2}$ orbital and one or more adjacent $O_{p\sigma}$ orbitals. Based on this, Hubbard three-band models have been developed that incorporate the planar Cu $d_{x^2-y^2}$ and the two $O_{p\sigma}$ orbitals per CuO_2 plane (see Fig. 2a) [26,27].

Band calculations on doped cuprate systems led to a highly dispersed partially filled band of states having mixtures of Cu $d_{x^2-y^2}$ and $O_{p\sigma}$ character and leading to local B_{1g} character ($x^2 - y^2$) at the Fermi energy [28].

While the closed shell singlet $\text{Cu}^{\text{III}} d^8$ state originally proposed by Anderson [24,25] is energetically unfavorable, an effective singlet state can be formed from the hybridization of the Cu $d_{x^2-y^2}$ with the delocalized B_{1g} combination of the four adjacent $O_{p\sigma}$ orbitals. This is referred to as the Zhang-Rice singlet and is the basis for the reduction of the three-band Hubbard models to the popular single-band t - J model of superconductivity [29]. In the t - J Hamiltonian, originally proposed by Anderson [24,25], an empty $d_{x^2-y^2}$ orbital can hop to adjacent sites with matrix element t while the neighboring d^9 spins are AF coupled (J), as shown in Fig. 5. There is a final constraint that two such holes cannot reside on the same site (due to an on-site Coulomb repulsion).

A more general Hamiltonian actively studied as a potential model for understanding superconductivity in cuprates is the $t + U$ Hubbard model [30]. In addition to assuming that doping leads to Zhang-Rice singlet holes, with the hopping matrix element of t for a $d_{x^2-y^2}$ spin to hop to a neighboring site, this model includes a finite Coulomb repulsion, U , when two spins are on the same site.

Generalizations of these two models that include further hopping matrix elements have also been considered [29].

Many attempts to use such Hamiltonians to explain the superconductivity and/or the unusual properties of the normal states have been reported. An excellent short summary of these various theories of cuprates is contained in the book *Quantum Liquids* by Leggett [31]. A detailed exposition of many of these theories can also be found in the book *Handbook of High Temperature Superconductivity* edited by Schrieffer and Brooks [32].

These t - J and related Hamiltonians have not yet led to a plausible explanation of the many unusual properties of the cuprate superconductors. The current consensus is that these materials

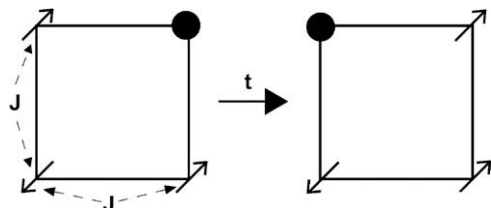


Fig. 5. Hamiltonian for the t - J model of cuprates. Neighboring d^9 spins are antiferromagnetically coupled with the undoped Heisenberg coupling $J = 0.13$ eV. The Zhang-Rice singlet 'hole' hops with matrix element t , but double occupancy of holes is forbidden [29]. Generalizations of the t - J model in the literature include additional hopping terms, such as diagonal hopping, t' . In other models, double occupancy of the spins is allowed with a Hubbard on-site Coulomb repulsion U and spin hopping matrix element t [30]. These models may be called ' $t + U$ -type' models.

have strongly correlated electrons and that new methods need to be developed to understand the nature of the ground state and its excitations.

3. New paradigm for the hole character from quantum mechanics

3.1. The proper description of the undoped antiferromagnetic insulator requires the B3LYP level of DFT

We mentioned above that band calculations for the doped cuprates have the holes in a highly dispersive band with Cu $d_{x^2-y^2}/O_{p\sigma}$ character, providing the basis for the t - J and $t + U$ models. A major catastrophe for these models is that, for undoped La_2CuO_4 , the same **band calculations lead to a metallic state with zero band gap [28,33,34] even though La_2CuO_4 is a semiconductor with an experimental band gap of 2.0 eV [35]!** This was rationalized as merely the common problem of density functional theory (DFT) leading to too small a gap.

In fact, this problem was only due to the flavor of DFT being applied. In 2001, we reexamined the band states of La_2CuO_4 using the B3LYP flavor of DFT, popular for QM of finite clusters and found that B3LYP leads correctly to an insulating ground state with the correct bandgap of 2 eV [36] without adding ad hoc self-interaction corrections [37–40]. The problem in describing the correct insulating AF ground state of La_2CuO_4 is that the system requires localized singly occupied $d_{x^2-y^2}$ orbitals, whereas methods such as LDA and PBE that do not include exact HF exchange (which is included in B3LYP) are inadequate to describe such states.

We have also used B3LYP to compute the electronic structure of undoped $\text{YBa}_2\text{Cu}_3\text{O}_6$, $\text{Tl}_2\text{Ba}_2\text{CaCu}_2\text{O}_8$, and the electron doped infinite layer SrCuO_2 [41]. In all of these cases, B3LYP correctly finds an insulating state with the correct band gap and AF coupling of the Cu. Recently, the $\text{CaCl}_2\text{CuO}_2$ cuprate has been calculated with similar results [42].

3.2. B3LYP leads to out-of-plane holes for doped systems

Given the success of B3LYP for the undoped system, we applied B3LYP to determine the electronic structure for the superconducting phase for the explicitly doped $\text{La}_{2-x}\text{Sr}_x\text{CuO}_4$ cuprate material [43]. Our previous cluster QM calculations using B3LYP suggested that doping would lead to out-of-the-plane holes [44,45].

To determine the band structure for the doped system, $\text{La}_{2-x}\text{Sr}_x\text{CuO}_4$, we considered $x = 0.125$ (which is close to the optimal doping of $x \approx 0.16$) and calculated the optimum wave function and geometry for the supercell, $\text{La}_{15}\text{SrCu}_8\text{O}_{32}$ (using the $2\sqrt{2} \times 2\sqrt{2} \times 1$ supercell with the maximum separation of Sr dopants). Calculations for $x = 0.25$ and 0.50 were also performed with identical results.

We found that the additional hole arising from doping with the Sr atom is localized along an O–Cu–O axis (z -direction) perpendicular to the CuO_2 plane with a mixture of Cu d_{z^2} character hybridized with the apical O p_z orbital as shown in Fig. 6 [43].

This result from B3LYP contrasts with the results from **all** previous DFT calculations (LDA and PBE) which, starting with the (incorrect) metallic description of the undoped system, found that the electrons are removed from the Cu/O $d_{x^2-y^2}/p\sigma$ band lying in the CuO_2 plane.

Out-of-the-plane holes from the best quality DFT calculations imply that **every prior theory** of cuprate superconductivity **used the wrong starting point** (holes in the CuO_2 plane). Thus, we had to start fresh to examine the impact of out-of-sheet holes on superconductivity. It took 5 years, but in 2007 we were able to show that these out-of-plane holes lead directly to the Chiral

Plaquette Polaron Paradigm (CPPP) that explains a broad spectrum of superconducting and normal state properties of the cuprates [46].

Our B3LYP QM calculations on doped $\text{La}_{2-x}\text{Sr}_x\text{CuO}_4$ [43] found two distinct but energetically similar states for the hole, as shown in Figs. 6 and 7:

- (1) the **apical** out-of-plane state in Fig. 6 has the hole shared over the O–Cu–O directly above the Sr. This singly occupied orbital prefers to be high spin coupled to the $d_{x^2-y^2}$ orbital on this Cu, leading to a local triplet state (the ground state of the $\text{Cu}^{\text{III}} d^8$ system),

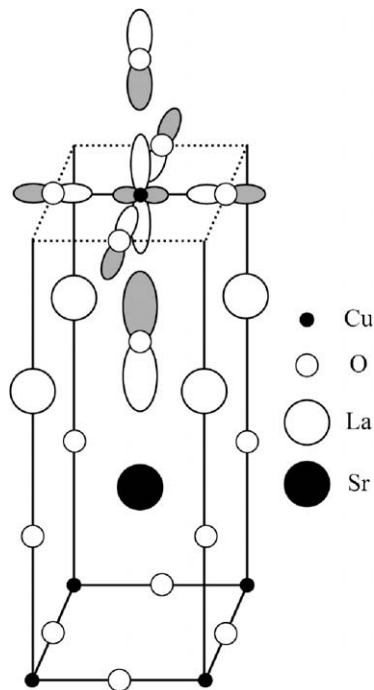


Fig. 6. The ‘apical’ polaron hole state found from B3LYP calculations of explicitly doped $\text{La}_{1.5}\text{Sr}_1\text{Cu}_8\text{O}_{32}$ ($x = 0.125$ doping) [43]. Density functionals that do not include exact Hartree–Fock exchange (LDA, GGA, PBE) do not find this out-of-the-plane hole state [28,33,34].

- (2) the **plaquette** state in Fig. 7 has the hole shared over the four $\text{Cu } d_{z^2}$ orbitals (and the two O atoms above and below each Cu) in a plane below the Sr dopant (each Cu is equidistant to the Sr). These four Cu also have four singly occupied $\text{Cu } d_{x^2-y^2}$ orbitals in the plane that were antiferromagnetically coupled for the undoped system. However, interaction with the delocalized out-of-plane hole frustrates this AF coupling leading to a more normal delocalized MO description of these $d_{x^2-y^2}$ in-plane orbitals.

Both states lead to distortions of the lattice near the site of the hole. Thus for the apical state, the loss of one electron from the $(\text{O}p_z)^2(\text{Cu } d_{z^2})^2(\text{O}p_z)^2$ orbitals of the out-of-plane O–Cu–O, leads to increased bonding and a decrease in the Cu–O out plane bond from $\sim 2.4 \text{ \AA}$ to 2.14 \AA for the apical state. Similarly, the plaquette state leads to a decrease of this out-of-plane Cu–O distance to 2.3 \AA . Because of these local distortions induced by the dopant hole, we refer to these states as **polarons**.

The current B3LYP calculations do not yet establish that the plaquette is more stable than the apical state. We have been optimizing the structures for both apical and plaquette, but the calculations are slow to converge because of the complexities due to the antiferromagnetic coupling that can lock in metastable pairs, the size (56 atoms per cell), and the very low symmetry. Our current B3LYP calculations find the plaquette state to be $0.053 \text{ eV} = 1.2 \text{ kcal/mol}$ above the apical state. This relative stability might be affected by the spin coupling states of the d^9 Cu, which depends on the cell size. This separation may also be sensitive to the DFT functional (for example it would be interesting to try the new M06 functionals [47]).

As discussed below, we have shown that the plaquette state leads to a self-consistent theory of the cuprates that explains the superconductivity and most of the puzzling experimental properties of these systems. However, our analysis indicates that *the apical hole would not lead to superconductivity*. In fact, while the apical state cannot occur in all cuprates (YBCO for example), all cuprates have structures that can lead to plaquette polarons. Thus, an assumption in our theory is that the plaquette state is the most stable (even though the current B3LYP calculations put the plaquette state 1.2 kcal/mol per 8 unit cells higher).

While the QM calculations on LSCO and YBCO lead to plaquettes in which the hole is delocalized between the Cu d_{z^2} and one or two out of plane O atoms (apical O), there are superconducting cuprates

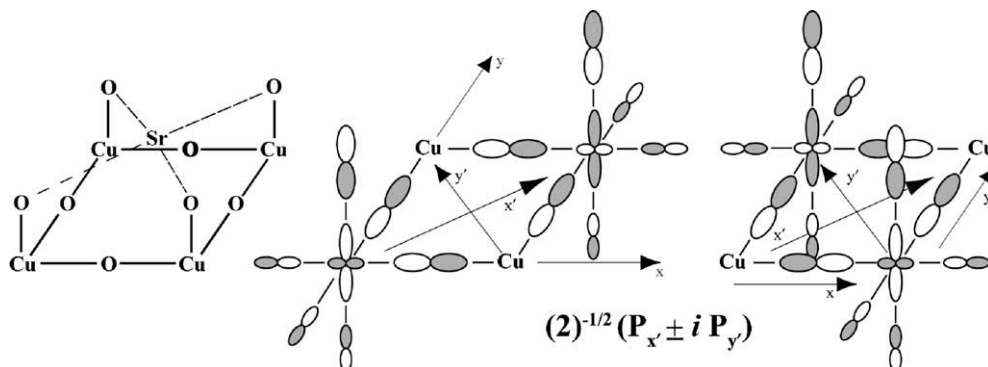


Fig. 7. The orbital view of the out-of-the-plane plaquette polaron hole state found from B3LYP calculations of explicitly doped $\text{La}_{1.5}\text{Sr}_1\text{Cu}_8\text{O}_{32}$ ($x = 0.125$ doping) [43]. Density functionals that do not include exact Hartree–Fock exchange (LDA, GGA, PBE) do not find this out-of-the-plane hole state [28,33,34]. Here, the Sr dopant centered above the four-site Cu plaquette shown in the left figure induces a hole that is distributed among the four out-of-the-plane apical O p_z , Cu d_{z^2} orbitals. Each of these can have some the local hole character in the A_{1g} combination of $\text{O}p_z$ orbitals for the in-plane O atoms. This plaquette leads to two degenerate states, P_x and P_y shown in the right two figures. Each of these states couples to the undoped Cu d^9 spin background neighboring the plaquette. Here P_x goes with one combination of antiferromagnetically coupled states and P_y goes with the other combination. We argued [46] that coupling these states to the spin background of d^9 states leads to a Jahn–Teller distortion that split the degeneracy to form *chiral* eigenstates with linear combinations $P_x \pm iP_y$ as the (with the corresponding combination of Cu d^9 spin background states). The complex phase factor, $\pm i$ implies that there is a net anti-clockwise or clockwise current in this state. This plaquette state would form on the bottom CuO_2 plane in Fig. 6.

with no apical O atoms in the ordered structure. Our CPPP theory **does not require the existence of apical O atoms**. Instead, we require the existence of a four-site plaquette comprised of orbitals orthogonal to the standard Cu/O $x_2y_2/p\sigma$ orbitals. In fact, a four-site plaquette comprised of **planar** $O_{p\pi}$ (see Fig. 4b) is sufficient to explain cuprate phenomenology (of course, this is not the ground state for the LSCO and YBCO systems). We generally refer to the plaquette hole in terms of out-of-the-plane O–Cu–O orbitals since this is what the QM leads to for the systems studied, but this restriction is not required.

All cuprates have disorder that may localize a four-site plaquette orthogonal to $x_2y_2/p\sigma$. For example, the electron-doped superconductor, $Nd_{2-x}Ce_xCuO_{4-\delta}$ ($T_c \sim 24$ K), has no apical O atoms, but it is known that O vacancies and an impurity phase, Ce_2O_3 , are necessary for the existence of superconductivity [48]. Similarly, the infinite-layer superconductor, $Sr_{1-x}La_xCuO_2$, has no apical O atoms in the ordered structure, but vacancies and impurity phases are expected [48]. For the hole-doped, materials $Bi_2Sr_2Ca_{n-1}Cu_nO_{4+2n}$, $TlBa_2Ca_{n-1}Cu_nO_{3+2n}$, $Tl_2Ba_2Ca_{n-1}Cu_nO_{4+2n}$, and $(Hg_{0.2}Tl_{0.8})Ba_2Ca_2Cu_3O_{8.33}$, superconductivity occurs due to excess O atoms in the material that resides out-of-the CuO_2 planes. This can localize a plaquette state.

Fig. 7 shows a degenerate pair of plaquette states denoted as P_x and P_y . These states can also be combined into the degenerate chiral combinations, $E^+ = P_x + iP_y$ and $E^- = P_x - iP_y$. As discussed below, we assume that the interaction of these states with the background of d^9 undoped spin throughout the lattice leads to a Jahn–Teller distortion that favors the chiral combinations.

Aside from the single Cu for the apical state or the four Cu associated with the plaquette, all other Cu atoms are the usual $Cu^{II} d^9$ sites with a single unpaired $d_{x^2-y^2}$ orbital that is superexchange coupled with the neighboring d^9 Cu sites with the undoped coupling, $J_{dd} = 0.13$ eV. We denote these Cu sites, the **undoped sites**.

We developed the Chiral Plaquette Polaron Paradigm (CPPP) [46] for cuprate superconductivity based on the insight from QM that doping leads to localized impurity states formed from out-of-the-plane orbitals. There are three different types of electrons in CPPP:

- (1) The usual undoped Cu $d^9 d_{x^2-y^2}$ singly occupied orbitals at the undoped sites that couple antiferromagnetically with $J_{dd} \approx 0.13$ eV ≈ 1500 K. These localized electrons are shown by the green and black dots in Fig. 8.
- (2) An out-of-the-plane plaquette polaron in the vicinity of each dopant. This doubly degenerate state involves one out-of-plane hole shared among the four Cu of the polaron. These electrons are shown by the red and blue squares in Fig. 8, indicating surface and interior plaquettes, respectively.
- (3) The four in-plane Cu/O $d_{x^2y^2}/p\sigma$ electrons inside the plaquette squares. A cross is used to represent these electrons inside some of the plaquettes, although they are present inside every plaquette in Fig. 8.

4. The Chiral Plaquette Polaron Paradigm (CPPP) of Cuprate Superconductivity

4.1. Fundamental assumptions

The basic assumptions of the CPPP are:

- (1) There are three types of electrons as described above. They are the undoped Cu d^9 electrons, the out-of-the-plane plaquette state that is delocalized over the four doped Cu sites, and the four in-plane Cu/O $d_{x^2y^2}/p\sigma$ orbitals of the plaquettes.

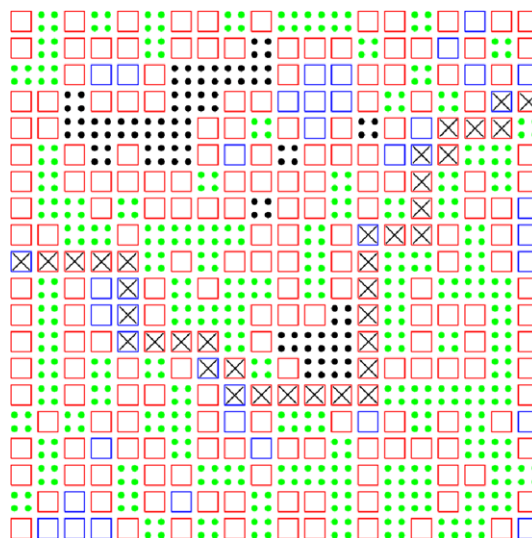


Fig. 8. One instance of the distribution over a 40×40 lattice of the plaquettes calculated for $x = 0.16$ doping. The squares represent the four-site plaquettes and the dots are the undoped Cu d^9 sites that couple antiferromagnetically ($J_{dd} = 0.13$ eV) with neighboring sites. There are $40^2 \times 0.16 = 256$ plaquettes in the figure. Here, we find two types of plaquettes: surface (red squares) and interior (blue squares). Note that the antiferromagnetic undoped d^9 islands are completely surrounded by plaquettes. It is the energy gap between the ground state singlet of these AF clusters and its first excited triplet state that is responsible for the '41 MeV' neutron spin resonance peak at the AF commensurate wavevector (π, π) . Three 4-site, one 24-site, and one 64-site AF clusters are highlighted with black dots. The black crosses indicate one percolating pathway for the four electrons in Cu $d_{x^2-y^2}$ orbitals within the plaquettes. Beyond the doping (0.05) at which the plaquettes percolate in 3D, we assume these electrons delocalize to form the canonical Cu/O $d_{x^2-y^2}/p\sigma$ band seen in photoemission spectroscopy. These band electrons delocalize over all the plaquettes in the percolating swath rather than over just the particular set of crosses shown.

- (2) Above the doping at which the four-site plaquette states percolate in 3D throughout the crystal, we expect the Cu/O $d_{x^2y^2}/p\sigma$ electrons inside the percolating swath to delocalize, forming a band. The band states are delocalized inside the red squares in Fig. 8 and then coupled to the corresponding states in adjacent plaquettes. We consider that this is the band observed in ARPES and expect that it is well characterized by LDA [28] and B3LYP [36] calculations. Thus, the LDA band structure, while incapable of describing the AF insulating state and the doping induced hole, may still be relevant for the cuprates. The LDA type band structure is formed **only** within the percolating metallic swath.
- (3) The plaquette states on the surface (shown by the red squares in Fig. 8) of the metallic swath are in contact with the undoped Cu d^9 spins, making them chiral, as discussed below and shown in Fig. 7. These chiral states carry an anti-clockwise or clockwise current around the four Cu sites that depends on the \pm phase between the two states the figure. We show below that the interaction of the delocalized Cu/O $x_2 - y_2/p\sigma$ band with the chiral plaquettes leads to D-wave superconducting pairing. For any particular plaquette, the local environment of the undoped d^9 spins in the vicinity of the plaquette, will generally split the degeneracy, leading to an energy difference between the two chiral states. This energy difference plays the same role as the Debye energy in the electron-phonon pairing in BCS superconductors. The interior plaquettes (shown by blue squares in Fig. 8) that do not neighbor undoped Cu d^9 spins, are **not** chiral.

- (4) Due to the random distribution of dopants in the crystal, the environment for each surface plaquette will be different. We assume the probability distribution of the anti-clockwise and clockwise plaquette energy splitting is uniform up to the maximum value, which is several J_{dd} (several thousand Kelvin).

The plaquette leads a two-fold degenerate polaron state $[(P_x, P_y)$ or $(E^+, E^-)]$ in the background AF d^9 spin environment. They are shown in Figs. 7 and 9. CPPP makes an additional assumption that goes beyond the results of our current ab-initio calculations. We assume that the interaction of the P_x and P_y states with the undoped Cu d^9 electrons leads to a Jahn–Teller distortion of the d^9 AF spin background that breaks the degeneracy of the E_x and E_y plaquette states, leading to the $E_+ = P_x + iP_y$ and $E_- = P_x - iP_y$ chiral combinations as the plaquette ground state. This phenomenon was derived for the t - J Hamiltonian [49–51] by an analysis that applies to our system. This chiral plaquette leads to an electron current moving clockwise or counter-clockwise inside the plaquette. As the system is doped, the plaquettes eventually percolate through the crystal while the Cu $d_{x^2-y^2}/O_{p\sigma}$ band electrons delocalize over this swath.

4.2. The Hamiltonian

In CPPP, the Hamiltonian describing the system reduces to a spin Hamiltonian of the form

$$H_{\text{tot}} = H_{\text{dd}} + H_{\text{pd}} + H_{\text{ch}}, \quad (2)$$

where H_{dd} describes the (AF d^9)–(AF d^9) spin coupling as in (1), H_{pd} describes the (AF d^9)–(polaron) spin coupling, with sums over terms like $J_{\text{pd}} S_p \cdot S_d$ where S_p is the plaquette polaron spin and S_d is the spin of an undoped d^9 spin. As shown in detail [46], H_{ch} describes the chiral coupling of the plaquette with the neighboring d^9 spins, with sums over terms like $\pm J_{\text{ch}} S_p \cdot (S_{d1} \times S_{d2})$ where the \pm sign depends on the chirality of the plaquette. This coupling of three spins arises from the circulating current in the plaquette and leads to non-coplanar d^9 spins. Under time reversal, $|P_x + iP_y\rangle \rightarrow |P_x - iP_y\rangle$, $J_{\text{ch}} \rightarrow -J_{\text{ch}}$, and $S_p \rightarrow -S_p$. Thus, H_{ch} and H_{dd} are time reversal invariant while H_{pd} changes sign

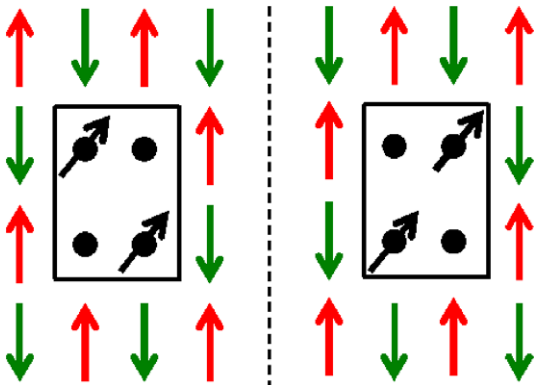


Fig. 9. Schematic drawing of the P_x and P_y degenerate plaquette states with the undoped Cu d^9 spin background shown. These spin backgrounds are incompatible and we expect a Jahn–Teller distortion analogous to that calculated in the t - J model to occur that distorts the background d^9 spins to form chiral linear combinations $E_+ = P_x + iP_y$ and $E_- = P_x - iP_y$. These can carry current around the plaquette. The background d^9 spins will split the degeneracy of these two states. This energy splitting is expected to be random and uniformly distributed throughout the surface plaquettes in the crystal. The energy splitting between these two time-reversed plaquettes states is proportional to the undoped AF spin coupling, $2J_{\text{dd}} \approx 0.26$ eV as described in Section 4.2. It plays the role filled by the Debye energy in BCS superconductors, but is much larger, leading to higher T_c 's.

$$J_{\text{pd}} S_p \cdot S_d \rightarrow -J_{\text{pd}} S_p \cdot S_d. \quad (3)$$

From Eq. (3), H_{pd} splits the energy between time-reversed chiral polarons. The energy difference between time-reversed plaquettes may be estimated in the following way: the AF coupling of the d_{z^2} orbital with a neighboring d^9 is $J_{\text{pd}} \sim J_{\text{dd}}$. There are 8 d^9 spins surrounding a plaquette. Since the out-of-plane spin in the plaquette orbital has a 1/4 probability to be on each Cu site, the energy splitting is on the order of $\sim (8/4) J_{\text{dd}} = 2J_{\text{dd}} \sim 0.26$ eV. The energy difference between polarons with the same spin but different chiralities is on the order of $4J_{\text{ch}} \sim 1$ eV.

The maximum energy splitting of $2J_{\text{dd}}$ for time-reversed plaquettes is important because it is the CPPP equivalent of the Debye energy in the BCS theory of classical superconductors [4]. This energy times the density of states at the Fermi level, is approximately the number of electrons that participate in superconducting pairing. If more electrons participate in pairing, then the superconducting state is more stable relative to the normal state. This leads to a higher T_c . In Section 6, the maximum T_c is estimated to be in the range of 0.05 to 0.15 times $2J_{\text{dd}}$, or 150 K to 450 K.

Based on the above assumptions, we developed a consistent theory of superconductivity of the cuprates that explains a large number of the puzzling and unique properties of these systems [45]. Some of these experiments and explanations are summarized in the next section.

5. Summary of experiments explained by the Chiral Plaquette Polaron Paradigm

This section describes some of the cuprate phenomenology explained by the CPPP [46]. An excellent short summary of cuprate phenomenology may be found in [31] and the references therein.

Three important universal features of cuprates can be understood using only the first two assumptions in Section 4 along with some simple counting arguments. These are the universal T_c phase diagram (Section 5.1), the universal room-temperature thermopower (Section 5.3), and the so-called ‘41 meV’ neutron spin resonance peak (Section 5.4). Section 5.2 explains the D-wave gap symmetry, 5.5 the incommensurate neutron spin scattering, 5.6 the ω/T scaling of neutron scattering, 5.7 the $1/T$ dependence of Hall effect, 5.8 the linear scaling of electrical resistivity at optimal doping, 5.9 the optical scattering and mid IR absorption, and 5.10, the Angle-Resolved-Photoemission (ARPES).

5.1. Universal T_c phase diagram

For all cuprate superconductors, the T_c as a function of doping follows the universal T_c phase diagram in Fig. 10, which is fitted by

$$T_c/T_{c,\text{max}} = 1 - 82.6(x - 0.16)^2, \quad (4)$$

where $T_{c,\text{max}}$ is the maximum T_c of the material and x is the hole doping per Cu in CuO_2 planes [52,53]. Superconductivity first appears at $x \approx 0.05$ doping, T_c is optimal at $x \approx 0.16$, and the superconductivity disappears at $x \approx 0.27$ doping. These universal characteristics have not been explained by any previous theory, but they are understood easily in the CPPP.

Since each plaquette comprises four Cu sites in a plane, a doping of $x = 1/4$ would not leave any remaining undoped d^9 spins to create chiral plaquettes and superconducting pairing. Thus CPPP suggests that $T_c = 0$ above $x = 0.25$. This is close to the $x \approx 0.27$ observed experimentally, which might arise because of the somewhat random distribution of dopant atoms.

In CPPP, the onset of superconductivity occurs for the minimum doping at which the plaquettes percolate. Assuming that the Sr doping is random (except not at nearest neighbor La sites), we calculate that percolation occurs at $x \approx 0.066$ (corresponding to 26%

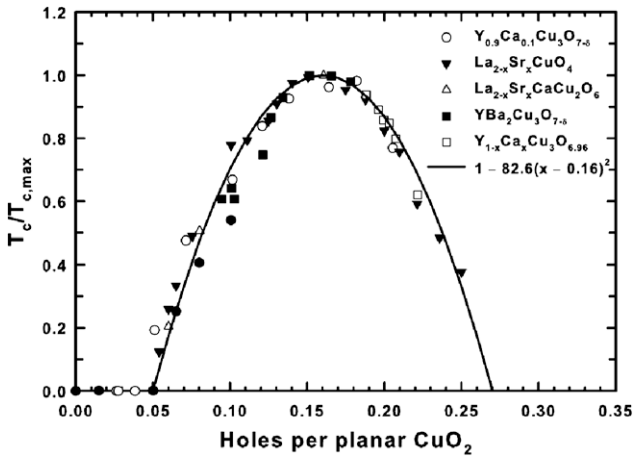


Fig. 10. The ratio of the superconducting temperature, T_c , to its maximum value $T_{c,max}$ as a function of doping in the CuO_2 sheets for several different cuprate classes. The solid line is the fit to the curve $(T/T_{c,max})=1 - 82.6(x - 0.16)^2$. Superconductivity begins at $x \approx 0.05$ hole doping per planar CuO_2 , is optimum at $x \approx 0.16$, and disappears at $x \approx 0.27$. The data is taken from Refs. [52,53].

of the sheet Cu in plaquettes) [46]. This is close to the observed onset of ≈ 0.05 . If we assume that plaquettes in neighboring CuO_2 planes are shifted by one Cu–O bond distance, as occurs in LSCO, BiSCCO, and TlBaCaCuO, then our calculated threshold for percolation becomes $x \approx 0.05$ [46].

In CPPP, the dependence of T_c on doping is controlled by the product of

- $N(0)$, density of states of the $\text{Cu}_{x-y/2}/\text{O}_{p\sigma}$ band, and
- V , the strength of the attractive pairing interaction,

because $N(0)V$ is the number of electrons near the Fermi level that can lower their energy due to Cooper pairing. $N(0)$ is proportional to the size of the metallic region per total volume in the material, while V is proportional to the number of surface plaquettes per total plaquettes (surface plus interior). Thus, the product $N(0)V$ is proportional to the number of surface plaquettes per total volume. Using a linear scaling percolation algorithm [54], we carried out simulations on 2000×2000 lattices assuming random doping of four-site plaquettes to find that the maximum surface plaquette to total volume occurs at $x = 0.167$ [46]. This is consistent with experiment, which finds a maximum T_c at $x \approx 0.16$ for all cuprate superconductors. Fig. 8 shows a typical distribution of plaquettes for a 40×40 lattice with $x = 0.16$.

Summarizing, the basic idea in CPPP of percolating plaquette polarons already explains the universal doping relation for the superconducting phase diagram as arising from surface area affects of the percolating metallic swath. No other theory explains these special doping values.

5.2. Symmetry of the superconducting gap

Consider a Cooper pair $(R\uparrow, R'\downarrow)$ with one electron at Cu site R with \uparrow spin and the other at site R' with \downarrow spin and consider the case in which both spins are part of the same four-site chiral plaquette. This Cooper pair can spin-exchange with itself through a second order spin-exchange by scattering the chiral plaquette from its initial state to its time-reversed state (opposite direction of current and opposite spin) and back. The matrix element describing this process is in Fig. 11. This leads to a spin-singlet repulsion when R, R' are on the same diagonal of the four-site plaquette and a spin-singlet attraction when they are nearest neighbors along a Cu–O bond direction. The reason the pairing has the opposite sign

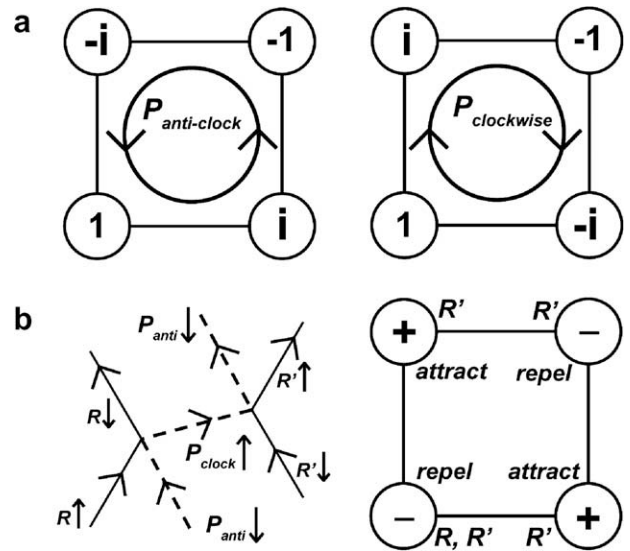


Fig. 11. Origin of D-wave superconducting pairing due to interaction an out-of-the-plane chiral plaquettes $(P_x + iP_y)$, with its time-reversed state, $(P_x - iP_y)$ (a) shows the phase relationship of an anti-clockwise current carrying plaquette and a clockwise current plaquette. The phase factor is $\pm i$ for neighboring Cu sites. (b) shows the second-order perturbation coupling between an $\text{Cu } d_{x^2-y^2}/\text{O}_{p\sigma}$ band electron with \uparrow spin at site R and an $\text{Cu } d_{x^2-y^2}/\text{O}_{p\sigma}$ band electron with \downarrow spin at site R' in the same plaquette as R . The site R is taken to be the lower left Cu site in (b). The band electron $R\uparrow$ spin-exchange interacts with an anti-clockwise \downarrow spin plaquette and scatters to an $R\downarrow$ $\text{Cu } d_{x^2-y^2}/\text{O}_{p\sigma}$ electron and clockwise \uparrow spin plaquette. This clockwise intermediate plaquette spin-exchange scatters with the $R'\downarrow$ $\text{Cu } d_{x^2-y^2}/\text{O}_{p\sigma}$ electron and returns back to its original state. The net effect is the $\text{Cu } d_{x^2-y^2}/\text{O}_{p\sigma}$ band electrons change from $(R\uparrow, R'\downarrow)$ to $(R\downarrow, R'\uparrow)$. The matrix element for the first interaction in the diagram in (b) leads to a factor of 1. If R' is located on one of the diagonal sites, then the second matrix element is also =1. When R' is on one of the neighboring sites, the second matrix element = -1 due to the opposing chiralities of the plaquettes states. Thus the matrix element is +1 for Cooper pairs on the same diagonal and -1 when they are on neighboring sites. The denominator in the second-order coupling is always negative for scattering at the Fermi surface since the intermediate plaquette is higher in energy than the initial state. This leads to a net negative matrix element for coupling Cooper pairs on the same diagonal and a plus for coupling along the Cu–O bond directions. This corresponds to singlet repulsion for diagonal pairs and singlet attraction for Cu–O bond pairs as shown in (b). The superconducting gap will acquire a node along the diagonal direction to avoid the repulsion there and will be non-zero along the Cu–O bond directions to benefit from the pairing. Therefore the gap becomes D-wave. Phonon pairing in classical BCS superconductors leads to an S-wave gap symmetry.

for Cu–O bond direction pairs can be seen by assuming the electron at site R is in the lower left corner of Fig. 11. When R' is on the same diagonal, the phases of the anti-clockwise and clockwise plaquettes are the same, leading to a plus sign (repulsive). When R' is on the neighboring sites along a Cu–O bond direction, then the phase factors of the two plaquette states lead to a minus sign (attractive).

The system minimizes its energy by creating a superconducting gap that is non-zero along the Cu–O bond directions and zero along the diagonal directions. This leads to a gap that changes sign between the x -axis and y -axis. Thus the gap is D-wave as observed experimentally [16–18].

5.3. Room-temperature thermopower

The thermopower, or Seebeck effect, is the voltage that is induced by a temperature gradient [10,11,55]. It has units of Volts/Kelvin. Fig. 12 shows the experimental room temperature (290 K) thermopower of all cuprates [52,53]. It has a universal dependence on doping, decreasing from positive S below $x \sim 0.15$ to a negative S above. This universal thermopower has remained unexplained, but CPPP explains it simply as the sum of two effects.

The first contribution is from the electronic thermopower of the metallic swath at 290 K. To understand the doping dependence of this term, we use the Mott formula, $S_e(T) = (\pi^2 k^2 / 3e) T (d/d\varepsilon) \ln \sigma(\varepsilon)$, where k is the Boltzmann constant, e is the magnitude of the electron charge, T is the temperature, and $\sigma(\varepsilon)$ is the conductivity at energy ε . The derivative is evaluated at the Fermi energy [10,11,55]. $\sigma(\varepsilon)$ includes the density of states and the scattering time, $\tau(\varepsilon)$. Since the derivative of the logarithm of $\sigma(\varepsilon)$ appears in S_e , multiplicative changes to the density of states and scattering time from doping will not change S_e . Thus, $S_e(290 \text{ K})$ is a constant independent of doping. $S_e(290 \text{ K}) = -12.5 \mu\text{V/K}$ from experimental data in the ($x > 0.27$) non-superconducting (purely metallic) region [52,53].

The second term arises from magnon drag due to interaction of the Cu $d_{x^2-y^2}/O_{p\sigma}$ band electrons with magnons in the undoped Cu d^9 regions. Magnon drag is completely analogous to phonon drag [55–58] arising from heat transport by non-equilibrium phonon distributions due to an electron current. It is given by $S_{\text{mag}}(T) = f(m c^2 / e) (1/T) (\tau_{\text{mag}} / \tau_e)$ [56], where m is the electron mass, e the electron charge, c is the magnon spin-wave velocity, f is the fraction of band momentum dissipated into magnons, τ_{magnon} and τ_e are the scattering lifetimes of the magnons and electrons, and T is the temperature. $f \sim (S/\Omega_M)T$, where S is the surface area of the metallic region and Ω_M is its volume. The T factor arises from induced magnon emission. $1/\tau_e \sim T$ at room-temperature (linear resistivity). Magnon scattering arises from interaction with the plaquettes, leading to $1/\tau_{\text{mag}} \sim (S/\Omega_{\text{AF}})T$, where Ω_{AF} is the AF region volume. The T factor is, once again, due to induced magnon emission. The surface, S , and temperature, T , cancel out and lead to $S_{\text{mag}}(T) = S_{\text{magnon}}(\Omega_{\text{AF}}/\Omega_M) = S_{\text{magnon}}(1 - 4x)/4x$, where S_{magnon} is a constant.

Combining these two terms leads to

$$S(290 \text{ K}) = S_{\text{magnon}}[(1 - 4x)/4x] + S_e, \quad (5)$$

where x is the doping in the CuO_2 plane, $S_e = -12.5 \mu\text{V/K}$ is the metallic contribution, and $S_{\text{magnon}} = 27.6 \mu\text{V/K}$ is the single parameter in our fit to the experiments, shown in Fig. 11. No previous theory has explained this remarkable universal thermopower.

5.4. Neutron spin scattering

Neutron spin scattering in the superconducting state leads to a peak for optimally doped YBCO ($T_c = 92 \text{ K}$) at an energy of 41 meV and wavevector (π, π, π) that is commensurate with the undoped AF spin state [59–65]. For optimally doped BiSCCO, this peak is at 43 meV. In both cases, the peak decreases as the doping decreases. This peak is important because it implies the existence of an unknown set of magnetic excitations that sharpen in the superconducting state. Such a peak is not found in classical BCS superconductors. The origin of this ‘41 meV’ peak is currently a very active part of cuprate research because it is believed it is connected to the superconducting pairing mechanism [59–65].

One popular explanation is that the peak arises from (π, π) k -vector nesting of the cuprate Fermi surface and D-wave BCS superconducting coherence factors that enhance the magnetic susceptibility at this k -vector [66]. This is analogous to how the S-wave gap BCS coherence factors lead to NMR spin relaxation peak just below T_c (the Hebel-Slichter peak) [67]. This model can be parameterized to fit the peak value, but the magnitude of the peak is 10–100 times too small. It is claimed that the magnitude of the peak is enhanced by AF spin fluctuations, but this merely introduces an additional fitting parameter. Moreover, this model predicts that the peak increases as the doping decreases, which is exactly the opposite of experiment.

In CPPP, the neutron spin scattering is due to excitations of the undoped d^9 spin regions that are surrounded by the plaquettes. We have calculated this with **no** adjustable parameters, finding a cor-

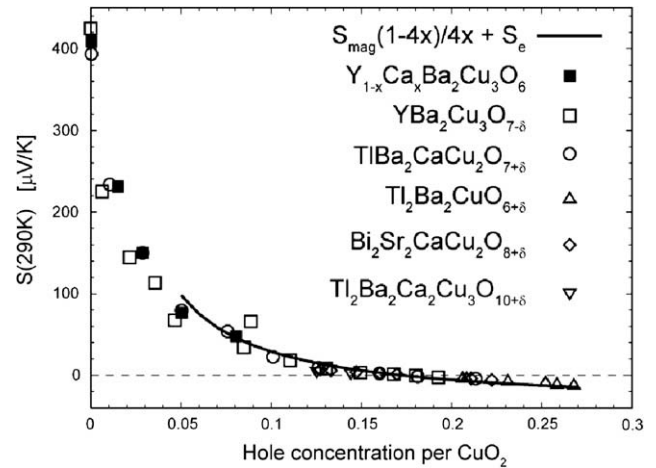


Fig. 12. One parameter fit of the experimentally observed universal room-temperature thermopower [52,53], or Seebeck coefficient, to the expression derived from the CPPP,

$$S(290 \text{ K}) = S_{\text{magnon}}[(1 - 4x)/4x] + S_e,$$

where $S_{\text{magnon}} = 27.6 \mu\text{V/K}$ is adjusted to fit experiment and $S_e = -12.5 \mu\text{V/K}$ is not adjusted. The first term in the expression arises from the magnon drag effect while the second term is the electronic thermopower contribution. The doping dependence of $S(290 \text{ K})$ is contained in the magnon drag contribution as explained in Section 5.4. Note that the thermopower goes to zero near $x = 0.16$, the optimal doping. For dopings below 0.05, the plaquettes do not percolate through the crystal and the Cu $d_{x^2-y^2}/O_{p\sigma}$ metallic band does not form. The thermopower below 0.05 is due to localized hopping, leading to a different form from our expression above.

rect value for the magnitude of the peak, a correct k -vector dependence, and a correct dependence on doping. To understand this phenomenon, note from Fig. 8, that the percolating plaquettes lead to undoped Cu d^9 islands completely surrounded by the plaquettes. These finite clusters are AF coupled (Heisenberg Hamiltonian, Eq. (1)) with the undoped spin-spin coupling, $J_{\text{dd}} = 0.13 \text{ eV}$. Since the cluster is finite in size, there is a finite gap between the singlet ground state to the first excited triplet state. This gap depends on the shape and size of the cluster. An excitation from the ground state to the triplet first-excited state will occur at the (π, π) commensurate k -vector and is the source of the neutron resonance peak.

Decreased doping increases the fraction of undoped d^9 sites making the finite clusters larger, leading to a smaller singlet-triplet excitation energy (this gap tends to zero for an infinite AF cluster). Thus the peak decreases with decreasing doping, in agreement with experiment.

We have calculated the gap energy for all AF cluster shapes and sizes up to 24 sites along with the neutron scattering matrix element. We computed the neutron scattering, from the distribution of cluster sizes at optimal doping obtained by randomly doping a large square lattice with plaquettes. We find that the peak occurs at 45.1 meV compared to experiment of 41 meV for YBCO and 43 meV for BiSCCO. The magnitude of the scattering is computed to be the same magnitude as the experiments. There are no adjustable parameters in the CPPP necessary to explain the 41 meV peak.

The reason that CPPP leads to a peak in the superconducting state is that the lifetimes of triplet AF cluster states are short due to interaction with the Cu $d_{x^2-y^2}/O_{p\sigma}$ band electrons surrounding the cluster. Below the superconducting T_c , a gap opens in the band structure that suppresses the decay of the triplet state. This would lead to a peak in the normal state, but we find that it is too broad to be distinguishable from the background.

Thus, the ‘41 meV’ peak is a signature of the inhomogeneity and percolation of the cuprates as computed in CPPP.

5.5. Incommensurate neutron spin scattering

In the normal state, the neutron spin scattering is incommensurate [9] and peaked at approximately $(\pi/a \pm 2\pi x/a, \pi/a)$ and $(\pi/a, \pi/a \pm 2\pi x/a)$ for low doping x where a is the Cu–Cu nearest neighbor distance. The peaks are shifted from the AF commensurate vector $(\pi/a, \pi/a)$ along the Cu–O bond directions with a magnitude that is proportional to the doping, x . This is surprising because the magnitude of the neutron spin scattering in metals is 100 times smaller than observed in cuprates and is extremely sensitive to the detailed shape of the Fermi surface. Thus, the simple relation observed in cuprates over a whole class of materials is unlikely to arise from metallic electron scattering of neutrons.

CPPP leads automatically to incommensurate scattering because of spin distortions arising from the chiral plaquettes states due to a circulating current. The chiral three-spin coupling, $\pm J_{ch} S_p \cdot (S_1 \times S_2)$ [46] involves the dot product of the plaquette spin S_p with the cross product of S_1 , and S_2 , the Cu d^9 spins neighboring the plaquette. The sign of the coupling is determined by the chirality of the plaquette. In essence, the chiral spin coupling, twists the AF spins such that they become non-coplanar and incommensurate. Our calculations find exactly the $2\pi x/a$ dependence observed experimentally [46].

The magnitude of neutron spin scattering scales as ω/E_{fermi} for metals and as ω/J for magnets, where E_{fermi} is the Fermi energy, J is the magnetic spin coupling, and ω is the energy change of the neutron. Since E_{fermi} is typically several eV and $J \sim 0.1$ eV, the incommensurate scattering in CPPP is larger than in metals. This magnitude is compatible with experiment, with the incommensurability arising from the localized d^9 spins coupling to the plaquettes.

5.6. ω/T scaling of neutron scattering

In a metal, the neutron scattering scales as $\chi'' \sim \omega/E_{fermi}$ where χ'' is the imaginary part of the magnetic susceptibility measured by neutron scattering, ω is the neutron energy change. In a magnet it scales as $\chi'' \sim \omega/J_{da}$.

In contrast, for cuprates the experimental neutron scattering exhibits an anomalous scaling relation, $\chi'' \sim \omega/T$, where T is the temperature [9]. This is completely unexpected because it implies that the cuprates have acquired a new energy scale that is proportional to temperature. The scaling is unexplained.

In CPPP, the random environment of each chiral plaquette leads to a uniform spread in the energy difference between an anti-clockwise and clockwise current-carrying plaquettes. This is assumption 4 above. Thus, at temperature T , there are $\sim T$ plaquettes that can scatter the neutron, leading to the scaling relationship. The new energy scale proportional to T arises from the number of plaquettes available at temperature T to scatter the neutron. A detailed analysis [46] finds that our computed χ'' is of the correct $\arctan(\omega/T)$ form found experimentally [9]. This explanation of the neutron scaling validates the existence of randomly split low-energy plaquette states in CPPP.

5.7. $1/T$ dependence of Hall effect

The Hall Effect measures the sign and magnitude of the charge carriers. For a normal metal, $R_H = 1/nec$, where n is the charge carrier density, e is the charge of the carriers (both magnitude and sign), and c is the speed of light. This expression is independent of T .

For cuprates, the Hall Effect in the normal state has a $1/T$ dependence at optimal doping [68]. This temperature dependence is too strong to be similar to a normal metal and too weak to be due to semiconducting behavior ($R_H \sim \exp(-\Delta/kT)$).

In CPPP, this $1/T$ dependence arises from the difference in the anti-clockwise and clockwise current carrying chiral plaquettes. In zero magnetic field, the number of anti-clockwise and clockwise plaquettes is the same. A finite field leads to additional skew-scattering (left-right asymmetry in scattering) contributions to the Hall Effect that is proportional to the difference in the number of the two types of plaquettes. This difference scales as $\sim 1/T$ (Curie-like contribution). For overdoped systems, the number of surface chiral plaquettes relative to the total number of electrons decreases, leading to a decrease of skew-scattering. Hence, the Hall Effect becomes weakly temperature dependent (like a metal) for overdoping, as is observed [68].

For magnetic fields in the CuO_2 plane, CPPP leads to a Hall Effect that is independent of T because an in-plane magnetic field does not affect the number of anti-clockwise and clockwise current carrying plaquettes because they carry circular current parallel to the CuO_2 planes. This is observed experimentally.

Thus, the anomalous temperature dependence of the Hall Effect in the cuprates provides a signature of the chirality of the plaquettes in CPPP.

5.8. Linear scaling of electrical resistivity at optimal doping

At low temperature a normal metal leads to a resistivity that is the sum of a constant due to impurity scattering plus a term that scales as T^5 (below $\sim 1/4$ the Debye temperature, or 50–100 K), whereas, at higher temperatures it is linear T due to phonon scattering (there are T phonons at temperature T due to the Bose-Einstein distribution of phonons). If the low temperature scattering was due to another kind of boson (magnons, for example), this same temperature dependence would still hold. The exponent in T^5 could change, but it must become a higher power than linear due to the loss of bosons at low temperatures from the Bose-Einstein distribution.

In contrast, the cuprates at optimal doping, exhibit a change in electrical resistivity with temperature that remains linear down to the lowest temperatures [69]. There is no evidence of the T^5 term and the constant impurity term is missing. This has never before been observed in metals and is considered a serious cuprate anomaly that a correct theory must explain.

The evolution of the temperature dependence of the resistivity of cuprates as a function of doping is also peculiar [69]. At low dopings, it increases approximately as T^2 at low temperatures, becoming linear at higher temperatures. At optimal doping, the resistivity is purely linear down to T_c . At higher doping, the resistivity evolves towards normal metallic behavior (due to electron–electron Coulomb scattering) as $x \rightarrow 0.3$. No evidence has ever been found of a phonon contribution.

In CPPP, the electrical resistivity arises from Coulomb scattering of Cu $d_{x^2-y^2}/O_{p\sigma}$ band electrons with the plaquette out-of-plane states. The uniform distribution of chiral plaquette energy splittings (that led to the neutron scaling described above) leads to the linear temperature dependence. The resistivity for underdoped materials is non-linear due to the pseudogap alteration in the density of states (discussed below in Section 5.10). The linear resistivity disappears for overdoped systems because only plaquettes on the surface with the undoped Cu d^9 spins contribute to the linear T term. Interior plaquettes formed in the overdoped region lead to additional impurity and electron–electron scattering contributions that scale as T^2 .

5.9. Optical scattering

Generalizing the CPPP argument for the linear resistivity to optical frequencies leads to a scattering rate of the form [46]

$$1/\tau \sim \max(\omega, T). \quad (6)$$

This reduces to a scattering rate proportional to T (linear resistivity) for $\omega = 0$. A scattering rate of this form leads to an anomalous optical reflectance spectrum at low temperatures and infrared frequencies of the form, $R = 1 - A\omega$, where A is a constant. This contrasts with the typical reflectance spectrum for a metal, which is given by the Hagen–Rubens relation, $R = 1 - A\omega^{1/2}$ [10,11]. The temperature and frequency scattering rate given by Eq. (6) is compatible with optical data on the cuprates [70].

In addition, an unexpected excess infrared absorption is observed that cannot be incorporated by any Drude-type relation using Eq. (6). The cuprates have a mid-IR absorption with a broad non-Drude peak at ~ 0.5 – 1.5 eV [70]. In CPPP this is due to photon transitions that flip plaquette chirality [46].

5.10. Angle-Resolved-Photoemission (ARPES)

For underdoped cuprates above T_c , a pseudogap is observed experimentally in the Angle-Resolved-Photoemission (ARPES) near $(\pi, 0)$ and $(0, \pi)$ [71]. This gap increases with decreased doping but vanishes for the overdoped systems ($x > 0.16$). This pseudogap is often cited as evidence that the electronic states of cuprates are not due to a Fermi liquid [71]. In fact, CPPP explains this pseudogap as due to the coupling of the $x_2y_2/p\sigma$ band inside the plaquette with the undoped Cu d^9 spins (more numerous for underdoped systems), which couples states having momentum differences near $(\pm\pi, \pm\pi)$. As the temperature increases, the magnitude of the (π, π) spin fluctuations in the undoped d^9 spins decreases, leading to a closing of the pseudogap as the temperature increases [46].

The anomalously large ARPES pseudogap and broad spectral functions for underdoped cuprates is due to the momentum k not being a good quantum number in the underdoped systems where the percolating metallic swath is ‘tortured’ and not translationally invariant [46].

6. Estimate of maximum T_c

An important question here is whether it is possible to obtain a T_c much above the current maximum of 138 K. To estimate the limits, consider the formula for T_c from BCS theory [67]

$$T_c = 1.13h\omega_D \exp(-1/N(0)V), \quad (7)$$

where $h\omega_D$ is the Debye energy, $N(0)$ is the density of states at the Fermi level, and V is the strength of the attractive coupling. In CPPP, the Debye energy is replaced by the scale of the energy splitting between opposite chirality plaquettes. As discussed in Section 4.2, the maximum energy for a plaquette surrounded on all four sides by d^9 spins is $\sim 2J_{dd} = 0.26$ eV ~ 3000 K. The maximum energy may range from 1/4 of the four-side maximum ($J_{dd}/2$) for the case in which one-side of the average plaquette has d^9 spin neighbors to 3/4 for the case in which the average plaquette has three-sides interfacing d^9 spin neighbors ($3J_{dd}/2$). Since the exponential term is $\sim 1/10$ for the A15 superconductors with $T_c \sim 23$ K, we suggest that the maximum possible T_c for a cuprate superconductor is in the range of $0.05J_{dd}$ to $0.15J_{dd}$ or 150 K to 450 K.

It is plausible that the current maximum of 138 K represents an average of one-side of each surface plaquette at the interface, which the above analysis estimates would lead to $T_c \sim 150$ K. Arranging the dopants such that the plaquettes have greater surface exposure to the undoped d^9 spins would increase the T_c , suggesting that a T_c of ~ 300 K might be attainable. Thus CPPP suggests that a great opportunity exists for new materials with improved properties.

7. Concluding remarks

A major revolution in materials science was the development of cuprate-based superconductors that, within the 8 years from 1986 to 1994, increased the maximum T_c from 25 K to 138 K. Clearly, there should be some overriding explanation of why these particular materials have such a high T_c and why they have a number of other unusual electronic and magnetic properties. However, an enormous effort by many different physics and chemistry groups failed to provide a theory that provides a convincing rationalization of most properties of these systems. We contend that the problem is that we, and all other theorists, were on the wrong track, due to the wrong assumption about the nature of the hole induced by doping.

Based on oversimplified QM calculations, we and others had believed that the doping responsible for superconductivity leads to holes in the CuO_2 planes. In 2001 we showed that the B3LYP flavor of DFT QM properly describes the 2 eV band gap of the undoped system (previous calculations using LDA and PBE led to a metallic undoped system) and in 2002 we showed that applying B3LYP to the doped system leads to holes that are localized on out-of-the-plane O–Cu–O regions near the dopant. In particular, we found a plaquette state in which the hole is localized over four neighboring O–Cu–O regions in a plane near the dopant. Based on this new paradigm, we published a paper in 2007 outlining our theory of superconductivity of these systems with very detailed discussions of each property [46].

This Letter attempts to provide a broader, chemically grounded explanation of the electronic states and of how the doping is related to the special properties. We find that very simple geometric arguments anchored in the 4-site nature of the plaquette can already explain much of the phenomenology. We hope that this will prove useful in developing new materials to improve the superconducting properties.

P.W. Anderson states [6],

‘I have always maintained that the correctness of a theoretical hypothesis is assured in this field if it can find a way to fit in with all these constraints: that there is likely to be only one possible way to fit all—or even a majority—of the observations together, and not to violate any theoretical impossibilities. In this process of fitting things together there is no room for one-experiment theories... The naked reality is strange enough.’

Indeed our model of out-of-the-plane orbitals interacting with undoped d^9 spins and Cu/O $x_2y_2/p\sigma$ band electrons does not ‘violate any theoretical impossibilities’ and explains the most experimental observations.

Finally, based on CCCP, we find that the T_c can be increased by controlling the location of the plaquettes, and that this could lead to $T_c \sim 300$ K (average of 2 interfaces to d^9 regions per plaquette) and perhaps $T_c \sim 450$ K (average of 3 interfaces to d^9 regions per plaquette). We hope that the plaquette ideas described here will help accelerate the development of improved materials with higher T_c .

References

- [1] J. Matricon, G. Waysand, C. Glashauser, *The Cold Wars: A History of Superconductivity*, Rutgers University Press, 2003.
- [2] P. Morel, P.W. Anderson, *Phys. Rev.* 125 (1962) 1263. The authors estimate the maximum electron-phonon pairing is $\lambda \approx 0.5$ and the Coulomb repulsion is $\mu \approx 0.1$ leading to an exponential factor in the BCS T_c expression of $\exp[-1/(\lambda - \mu)] \approx 0.08$. Multiplying by the Debye energy (~ 300 K) leads to $T_c \sim 30$ K. They do not actually do this final step. They stop at the λ and μ values.
- [3] J.G. Bednorz, K.A. Muller, *Z. Phys.* B64 (1986) 189.
- [4] J. Bardeen, L.N. Cooper, J.R. Schrieffer, *Phys. Rev.* 108 (1957) 1175.
- [5] P.W. Anderson, *The Theory of Superconductivity in the High- T_c Cuprates*, Princeton University Press, Princeton, New Jersey, 1997 (Chapter 2).

- [6] P.W. Anderson, *Low Temp. Phys.* 32 (2006) 282.
- [7] P.E. Sulewski, P.A. Fleury, K.B. Lyons, S.-W. Cheong, Z. Fisk, *Phys. Rev. B* 41 (1990) 225.
- [8] N.D. Mermin, H. Wagner, *Phys. Rev.* 22 (1966) 1133.
- [9] M.A. Kastner, R.J. Birgeneau, G. Shirane, Y. Endoh, *Rev. Mod. Phys.* 70 (1998) 897.
- [10] J.M. Ziman, *Principles of the Theory of Solids*, second edn., Cambridge, UK, 1972.
- [11] N.W. Aschcroft, N.D. Mermin, *Solid State Physics*, Holt, Rinehart, and Winston, New York, 1976.
- [12] Y. Guo, J.-M. Langlois, W.A. Goddard III, *Science* 239 (1988) 896.
- [13] G. Chen, W.A. Goddard III, *Science* 239 (1998) 899.
- [14] G. Chen, J.-M. Langlois, Y. Guo, W.A. Goddard III, *Proc. Natl. Acad. Sci.* 86 (1989) 3447.
- [15] W.A. Goddard III, Y. Guo, G. Chen, H. Ding, J.-M. Langlois, G. Lang, in: D.P. Tunstall, W. Barford, P. Osborne (Eds.), *High Temperature Superconductivity Proc. 39th Scottish Universities Summer School in Physics*, St. Andrews, Scotland, 1991.
- [16] C.C. Tsuei, J.R. Kirtley, *Rev. Mod. Phys.* 72 (2000) 969.
- [17] D.A. Wollman, D.J. Van Harlingen, W.C. Lee, D.M. Ginsberg, A.J. Leggett, *Phys. Rev. Lett.* 71 (1993) 2134.
- [18] C.C. Tsuei et al., *Phys. Rev. Lett.* 73 (1994) 593.
- [19] G. Chen, H.-Q. Ding, W.A. Goddard III, *Phys. Rev. B* 46 (1992) 2933.
- [20] H.-Q. Ding, G.H. Lang, W.A. Goddard III, *Phys. Rev. B* 46 (1992) 14317.
- [21] J. Tahir-Kheli, W.A. Goddard III, *Proc. Natl. Acad. Sci.* 90 (1993) 9959.
- [22] J. Tahir-Kheli, W.A. Goddard III, *Phys. Rev. B* 47 (1993) 1116.
- [23] J. Tahir-Kheli, W.A. Goddard III, *Phys. Rev. B* 48 (1993) 13002.
- [24] P.W. Anderson, *Science* 235 (1987) 1196.
- [25] P.W. Anderson, in: R.A. Broglia, J.R. Schrieffer (Eds.), *Frontiers and Borderlines in Many-Particle Physics: Varenna on Lake Como, Villa Monastero, 7–17 July 1987*, North Holland, Amsterdam, the Netherlands, 1988.
- [26] V.J. Emery, *Phys. Rev. Lett.* 58 (1987) 2794.
- [27] C.M. Varma, S. Schmitt-Rink, E. Abrahams, *Solid State Commun.* 62 (1987) 681.
- [28] W.E. Pickett, *Rev. Mod. Phys.* 61 (1989) 433.
- [29] F.C. Zhang, T.M. Rice, *Phys. Rev. B* 37 (1987) 3759.
- [30] D.J. Scalapino, in: J.R. Schrieffer, J.S. Brooks (Eds.), *Handbook of High-Temperature Superconductivity*, Springer, New York, 2007.
- [31] A.J. Leggett, *Quantum Liquids: Bose Condensation and Cooper Pairing in Condensed-Matter Systems*, Oxford University Press, Oxford, 2006.
- [32] J.R. Schrieffer, J.S. Brooks (Eds.), *Handbook of High-Temperature Superconductivity*, Springer, New York, 2007.
- [33] J. Yu, A.J. Freeman, J.H. Xu, *Phys. Rev. Lett.* 58 (1987) 1035.
- [34] L.F. Mattheis, *Phys. Rev. Lett.* 58 (1987) 1028.
- [35] J.M. Ginder, R.M. Roe, Y. Song, R.P. McCall, J.R. Gaines, E. Ehrenfreund, A.J. Epstein, *Phys. Rev. B* 37 (1988) 7506.
- [36] J.K. Perry, J. Tahir-Kheli, W.A. Goddard III, *Phys. Rev. B* 63 (2001) 144510.
- [37] K. Shiraishi, A. Oshiyama, N. Shima, T. Nakayama, H. Kamimura, *Solid State Commun.* 66 (1988) 629.
- [38] A. Svane, *Phys. Rev. Lett.* 68 (1992) 1900.
- [39] W.M. Temmerman, Z. Szotek, H. Winter, *Phys. Rev. B* 47 (1993) 11533.
- [40] M.T. Czyzyk, G.A. Sawtsky, *Phys. Rev. B* 49 (1994) 14211.
- [41] J. Tahir-Kheli, M.-J. Cheng, W. A. Goddard III, unpublished.
- [42] C.H. Patterson, *Phys. Rev. B* 77 (2008) 115111.
- [43] J.K. Perry, J. Tahir-Kheli, W.A. Goddard III, *Phys. Rev. B* 65 (2002) 144501.
- [44] J.K. Perry, J. Tahir-Kheli, *Phys. Rev. B* 58 (1998) 12323.
- [45] J. Tahir-Kheli, *Phys. Rev. B* 58 (1998) 12307.
- [46] J. Tahir-Kheli, W.A. Goddard III, *Phys. Rev. B* 76 (2007) 014514.
- [47] Y. Zhao, D.G. Truhlar, *Theor. Chem. Acc.* 120 (2008) 215.
- [48] H.J. Kang et al., *Nat. Mater.* 6 (2007) 224.
- [49] A.A. Belavin, A.M. Polyakov, *JETP* 22 (1975) 245.
- [50] X.G. Wen, F. Wilczek, A. Zee, *Phys. Rev. B* 39 (1988) 11413.
- [51] R.J. Gooding, *Phys. Rev. Lett.* 66 (1991) 2266.
- [52] J.L. Tallon, C. Bernhard, H. Shaked, R.L. Hitterman, J.D. Jorgensen, *Phys. Rev. B* 51 (1995) 12911.
- [53] S.D. Obertelli, J.R. Cooper, J.L. Tallon, *Phys. Rev. B* 46 (1992) 14928.
- [54] M.E.J. Newman, R.M. Ziff, *Phys. Rev. E* 64 (2001) 016706.
- [55] D.K.C. MacDonald, *Thermoelectricity: An Introduction to the Principles*, Wiley, New York, 1962.
- [56] C. Herring, *Phys. Rev.* 96 (1954) 1163.
- [57] L. Gurevich, *J. Phys. (U.S.S.R)* 9 (1945) 477.
- [58] H.J. Trodahl, *Phys. Rev. B* 51 (1995) 6175.
- [59] J. Rossat-Mignod et al., *Physica C* 185 (1991) 86.
- [60] H.A. Mook, M. Yethiraj, G. Aeppli, T.E. Mason, T. Armstrong, *Phys. Rev. Lett.* 70 (1993) 3490.
- [61] H.F. Fong, P. Bourges, Y. Sidis, L.P. Regnault, A. Ivanov, G.D. Gu, N. Koshizuka, B. Keimer, *Nature* 398 (1999) 588.
- [62] H.F. Fong et al., *Phys. Rev. B* 61 (2000) 14773.
- [63] G. Aeppli et al., *Phys. Rev. Lett.* 62 (1989) 2052.
- [64] P. Bourges, H.F. Fong, L.P. Regnault, J. Bossy, C. Vettier, D.L. Milius, I.A. Aksay, B. Keimer, *Phys. Rev. B* 56 (1997) R11439.
- [65] H.F. Fong, B. Keimer, D. Reznik, D.L. Milius, I.A. Aksay, *Phys. Rev. B* 54 (1996) 6708.
- [66] N. Bulut, D.J. Scalapino, *Phys. Rev. B* 47 (1992) 3419.
- [67] M. Tinkham, *Introduction to Superconductivity*, second edn., Dover, New York, 1996.
- [68] H.Y. Hwang, B. Batlogg, H. Takagi, H.L. Kao, J. Kwo, R.J. Cava, J.J. Krajewski, W.F. Peck, *Phys. Rev. Lett.* 72 (1994) 2636.
- [69] H. Takagi, B. Batlogg, H.L. Kao, J. Kwo, R.J. Cava, J.J. Krajewski, W.F. Peck, *Phys. Rev. Lett.* 69 (1992) 2975.
- [70] D.N. Basov, T. Timusk, *Rev. Mod. Phys.* 77 (2005) 721.
- [71] A. Damascelli, Z. Hussain, Z.-X. Shen, *Rev. Mod. Phys.* 75 (2003) 473.



Jamil Tahir-Kheli obtained a B.A. and M.A. in Mathematics from Oxford University (Oriental College). He has an M.S. and PhD (1992) in Physics from California Institute of Technology. From 1993 to 2001, he consulted in industry. A part of the consulting was in finance. He can confidently state that none of his models are responsible for the current state of the economy. Since 2001, he has been a Senior Staff Scientist at Caltech. His research interests are superconductivity, high ZT thermoelectrics, and ab-initio transport calculations.



William A. Goddard III is the Charles and Mary Ferkel Professor of Chemistry, Materials Science, and Applied Physics and Director of the Materials and Process Simulation Center at California Institute of Technology, where he has been on the faculty since 1965. His BS Engineering was from UCLA and his PhD in Engineering Science (minor physics) from Caltech. He develops new methodology for quantum chemistry, reactive force fields, molecular dynamics, and electron dynamics and applies these methods to atomistic simulations of chemical, biological, and materials systems, including catalysis (homogenous and heterogeneous), polymers, semiconductors, superconductors, and metal alloys. Particular interests are protein structure prediction, drug design, fuel cells, energetic materials, and nanoelectronics. He is a member of the National Academy of Sciences and winner of the 2007 ACS award in theoretical chemistry.